Journal of Electronic Imaging 14(3), 033010 (Jul–Sep 2005)

Multigradient field-active contour model for multilayer boundary detection of ultrasound rectal wall image

Di Xiao
National University Hospital
Department of Surgery
Singapore 169608
E-mail: MDXiao@ntu.edu.sg

Wan Sing Ng
Nanyang Technological University
School of Mechanical and Production Engineering
Computer Integrated & Medical Intervention Laboratory
Singapore 639798

Udantha R. Abeyratne
The University of Queensland
School of Info. Tech. & Electrical Eng
Brisbane Q1d 4072, Australia

Charles B. Tsang
National University Hospital
Department of Surgery
Singapore 169608

Abstract. *Extraction and reconstruction of rectal wall structures from an ultrasound image is helpful for surgeons in rectal clinical diagnosis and 3-D reconstruction of rectal structures from ultrasound images. The primary task is to extract the boundary of the muscular layers on the rectal wall. However, due to the low SNR from ultrasound imaging and the thin muscular layer structure of the rectum, this boundary detection task remains a challenge. An active contour model is an effective high-level model, which has been used successfully to aid the tasks of object representation and recognition in many image-processing applications. We present a novel multigradient field active contour algorithm with an extended ability for multiple-object detection, which overcomes some limitations of ordinary active contour models—"snakes." The core part in the algorithm is the proposal of multigradient vector fields, which are used to replace image forces in kinetic function for alternative constraints on the deformation of active contour, thereby partially solving the initialization limitation of active contour for rectal wall boundary detection. An adaptive expanding force is also added to the model to help the active contour go through the homogenous region in the image. The efficacy of the model is explained and tested on the boundary detection of a ring-shaped image, a synthetic image, and an ultrasound image. The experimental results show that the proposed multigradient field-active contour is feasible for multilayer boundary detection of rectal wall.* © *2005 SPIE and IS&T.*
[DOI: 10.1117/1.1992500]

1 Introduction

Endoscopic ultrasonography[1,2] (EUS) has become one of the common techniques for screening of the rectum and early staging of rectal tumors in the current clinical diagnosis, because of its advantage in providing a sequence of cross-sectional ultrasound images of the rectum.[3,4] On these cross-sectional images, the anatomical structure of the organs and the situation of potential tumors can be assessed. However, the problem with the current EUS machine is that the machine provides only a sequence of images displayed to a surgeon, thereby leaving much laborious follow-up work concerning image understanding and analysis for the surgeon to complete. For example, to extract structural information of the rectal wall and further the position information of the possible rectal tumor, a surgeon usually must view the ultrasound images slice by slice, and finally form a full structural picture of that rectum in his mind. The diagnostic result such as tumor staging[5–7] can be done only by this information built in his head.

Although some recent commercial products have had the ability to help surgeons visualize the 3-D ultrasound rectal image, to our knowledge, in the image-processing area, there are still no published methods on the extraction and analysis of the rectal wall structure. Today, even simple manual outlining of the method for rectal layer description is not applied in clinical practice. It is still a time-consuming and tedious work for surgeons to perform object recognition and information extraction. Thus, to develop a set of algorithm to help the information extraction of the anatomical structure of the rectum from an ultrasound image will be meaningful for reducing the surgeon's repetitive work.

Paper 03042 received Mar. 11, 2003; revised manuscript received Feb. 13, 2004; accepted for publication Dec. 14, 2004; published online Jul. 15, 2005.
1017-9909/2005/14(3)/033010/14/$22.00 © 2005 SPIE and IS&T.

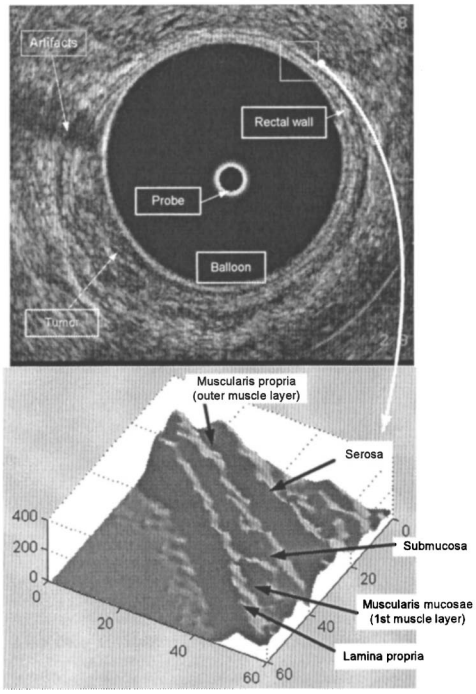

Fig. 1 Rectal ultrasound image.

Figure 1 shows a cross-sectional ultrasound image of a rectum with a tumor, which consists of three main parts: balloon area, rectal wall area, and tissue area. Today, with a 10-MHz ultrasonic probe, surgeons can distinguish five muscular layers of a rectal wall by their eyes from an unprocessed ultrasound image. These are the lamina propria, the muscularis mucosae (first muscle layer), the submucosa, the muscularis propria (second muscle layer), and the serosa. From the ultrasound image feature point of view, the central part is the balloon area with a gray-level value of low intensity. Five muscular layers can be distinguished by their different gray-level values. For example, the lamina propria has higher intensity than the muscularis mucosae layer, thus showing higher brightness.

For clinical application, rectal wall boundary detection, tumor detection, and further 3-D reconstruction of rectum and tumor staging is meaningful for intuitive 3-D visualization and quantitative analysis of the rectum and will be a grand goal. In this paper, our aim is to set up a feasible algorithm to perform the boundary detection of muscular layers of the rectum from its ultrasound image. The obtained data will be helpful for the further quantitative analysis and 3-D reconstruction, which will display a visual anatomical structure of the rectum for surgeons. The boundary detection of the rectal wall muscular layer is difficult because of the low resolution and contrast speckle structure of ultrasound images, and too thin a layer structure of the rectum. Therefore, conventional approaches, such as low-level edge detection, edge linking methods, etc., are not suitable for our task. Some other high-level methods for their specific uses may not meet our demand for multilayer detection of the rectal structure.[8,9]

Recently, the active contour model "snakes" is a much appreciated algorithm used by many researchers for boundary detection in image processing. The name "active contour" originated from the elastic theory in physics. The procedure of object matching is a searching procedure that uses the optimal approximation theory to obtain the energy minimum. The shape and the evolution progress of one active contour model have the characteristics of geometry, physics, and optimal approximation. After studying its performance, we found its basic characteristics meet the requirement of our goal. With the "snakes" method, the anatomical knowledge of the rectum can be integrated into the boundary-detecting procedures. And benefiting from the characteristic of closed contour, we can obtain a fully closed boundary that we required in this project though some parts on the layer's boundary may be lost. Further, the "snakes" method can implement the boundary detection and object recognition at the same time, which cannot be done by a low-level method.

The "snakes" algorithm was originally developed by Kass *et al.*[10] in 1987. After that, a series of papers on modification and improvement of the original snakes algorithm were published. Amini *et al.* pointed out some of the problems with this approach, such as instability and a tendency for points to bunch up a strong portion of an edge. They proposed an algorithm for the snakes model using dynamic programming.[11] This algorithm is more stable and enables the inclusion of hard constraints in addition to the soft constraints inherent in the formulation of the functional. Further, a fast algorithm called a "greedy algorithm" for snakes was proposed, which was stable, flexible, enabled hard constraints, and ran much faster than the dynamic programming method.[12] A finite-element algorithm was also used to make the solution of the model faster and more stable. Menet *et al.* gave a B-snake model, which was built from the initial curve approximation by a parametric B-spline.[13] Based on the elementary characteristics of B-spline, B-snake is capable of doing the local and continuity control and can solve the "corner" problem. A similar work based on B-spline can be found in Ref. 14. Cohen introduced a new model for snakes through adding a new external force, which makes the curve behave like a balloon to solve the "initial sensitivity problem."[15,16] Xu and Segawa gave a robust active contour model.[17] They highlighted a problem of the snake model in that the performance of the model depended on proper internal parameters and the initial contour position. To solve this problem, they proposed adding another energy term that could resist the internal normal force and make the contour keep still regardless of the current contour shape. Gradient vector flow is a novel method to solve the initial position problem.[18,19] The main characteristic of the gradient vector flow is that it extends the gradient map farther away form the edges and into homogeneous regions using a computational diffusion process algorithm. Cañero *et al.* used a generalized gradient vector flow biplane snakes in his coronary vessel application.[20] United snakes algorithm is a combination of the original snakes algorithm and live-wire algorithm to locate the initial position of an active contour.[21] The snakes in Ref. 22 aimed at solving the oscillating problem. There are also a many works to apply the snakes method on image segmentation,[23–25] motion tracking,[26–30] and matching.[31–33] In general, the algorithm improvement related to snakes mainly focused on the problems of stability, initialization, and convergence. For an over review, see Ref. 34.

We have known, because of some inherent limitations, that snakes can not solve the entire problem of finding contours in images; rather, they depends on other mechanisms such as interaction with a user, interaction with some higher level image understanding process, or information from image data adjacent in time or space. In our project, one problem is the initialization of the snakes. To detect the boundary of each layer, if a conventional algorithm was used, each initial position should be set manually in the capture range of each boundary. For example, for detection of six boundaries of five muscular layers of the rectum, six initial positions of the snakes should be set, which is a very time-consuming work for a surgeon. In this paper, we focus on how solving this kind of "initial problem."

In this paper, we propose a novel multigradient field active contour to solve the preceding limitations.[35,36] The following are contributions in this paper:

1. We propose a multigradient field concept and add it into the traditional snakes.
2. We propose a multigradient field algorithm, which is capable of multiple boundaries detection by an active contour given one initial position in our project.
3. We introduce a boundary detection technique into the anatomical structure extraction from sequence of rectal wall ultrasound images, which is helpful for clinical image understanding and further 3-D reconstruction of rectum structure from ultrasound images.

2 Method

Muscular layer detection of the rectal wall requires several tasks to be completed at the same time, including border detection and object recognition. Not only the current boundary must be detected, but there is also necessary to know which layer this boundary belongs to in a rectal wall image. An intuitive central thought in this paper is to first place an initial contour in the balloon area of the rectal wall, then deform this active contour and obtain the innermost layer's boundary, which is also called inner boundary of the first muscular layer. Using this boundary as the new model we continuously expand it to extract the outer boundary of the first layer (or inner boundary of the second muscular layer). Repeating the same approach, each layer can be detected progressively. The advantage of this method is that it can overcome the limitation of the conventional snakes algorithm that must place each initial contour in the capture range of each specific muscular layer boundary.

Through analyzing the gradient vector field of the rectal wall image, we found the whole procedure of extracting the boundaries is more complicated than it appears to be. Actually, the active contour model must have the capability to solve such more complicated problems. It must have the capability to solve such problem as

1. In a homogeneous region like the balloon area, how do we deform the active contour model to enter the gradient capture range of the inner boundary?
2. How do we control the deformation of the model and carefully make it not cross each layer or escape from the attraction of the gradient field?
3. When using a current obtained boundary as a new model to search for the next layer, how do we overcome the attraction of the current gradient field?

For solving all these problems, a novel boundary detection method is proposed for the realization of the muscular layer detection of rectal wall.

2.1 *Multigradient Field-Active Contour Model*

Here, a novel active contour model based on the framework of traditional active contour model snakes is set up. The energy function of the improved active contour E_{IAC} is defined as follows:

$$E_{\mathrm{IAC}} = \int E_{\mathrm{int}}[\mathbf{v}(s)] + w_{\mathrm{image}} E_{\mathrm{image}}[\mathbf{v}(s)] + w_{\mathrm{adpt}}[\mathbf{v}(s)] E_{\mathrm{adpt}}[\mathbf{v}(s)]\, \mathrm{d}s, \tag{1}$$

where $\mathbf{v}(s)=[x(s),y(s)]$ represents parametric vector of the active contour model, s is the arc length of the contour, w_{image} and w_{adpt} are weights, and E_{int} is an internal energy of the active contour. This term is the same as that in the traditional snakes, which is used to compose the regularity of the curve. Here E_{image} is image energy, which is an external constraint that comes from the image features so that it takes on its smaller values at the features of interest. The force derived from it is constrained by our multigradient field, which is totally different from that in the traditional snakes. Adaptive expanding energy E_{adpt} is an external energy. The corresponding force derived from it can make the active contour model expand with an adaptive feature. This is strongest in the homogenous region that has no gradient field, and smallest when near to the desired edges. Detailed features of the last two energy terms will be explained in the following three subsections.

2.2 *Numerical Solution of the Multigradient Field Active Contour Model*

The goal of the solution to the model is to find a contour that minimizes Eq. (1) driven by the internal energy, image energy, and expanding energy. In this paper, we choose using the kinetic function rather the preceding energy function to deform the active contour, thus we should get the corresponding force equation as well as its corresponding numerical solution. By using the calculus of variations and solving the Euler equations, we can give the minimization of Eq. (1). Because the form of our energy function is similar to snakes, the numerical solution procedure is the same. Here, we just list several important equations to facilitate further discussion. The detailed procedure of numerical solution can be found in Ref. 10.

The Euler equations obtained from the Eq. (1) can be described as following two dependent parts, assuming that $\alpha(s)$, $\beta(s)$, $w_{\mathrm{image}}[\mathbf{v}(s)]$, and $w_{\mathrm{adpt}}[\mathbf{v}(s)]$ are constant:

$$\frac{\partial}{\partial s}\left(\alpha\left|\frac{\partial x(s)}{\partial s}\right|\right) - \frac{\partial}{\partial s^2}\left(\beta\left|\frac{\partial^2 x(s)}{\partial s^2}\right|\right) - w_{\mathrm{image}}\frac{\partial E_{\mathrm{image}}(x,y)}{\partial x} - w_{\mathrm{adpt}}\frac{\partial E_{\mathrm{adpt}}(x,y)}{\partial x} = 0, \tag{2a}$$

$$\frac{\partial}{\partial s}\left(\left|\frac{\partial y(s)}{\partial s}\right|\right)-\frac{\partial}{\partial s^2}\left(\left|\frac{\partial^2 y(s)}{\partial s^2}\right|\right)-w_{\text{image}}\frac{\partial E_{\text{image}}(x,y)}{\partial y}-w_{\text{adpt}}\frac{\partial E_{\text{adpt}}(x,y)}{\partial y}=0. \tag{2b}$$

Finite differences are used to approximate the first and second differential terms of a function. Substituting these in Eqs. (2a) and (2b) and minimizing the energy function of the active contour, a pair of systems of the equations for finding x and y coordinates can be achieved. Each node on the active contour can be converted to a vector notation with $\mathbf{v}_i=(x_i,y_i)$. The active contour is made dynamically by treating each vector $\mathbf{v}_i$ as the function of time t.

By an explicit Euler method, the final solutions of the Eqs. (2a) and (2b) can be expressed in matrix forms as follows:

$$x_t=(\mathbf{C}+l\mathbf{I})^{-1}[lx_{t-1}-w_{\text{image}}f_{\text{img\_}x}(\mathbf{x}_{t-1},\mathbf{y}_{t-1})+w_{\text{adpt}}f_{\text{adpt\_}x}(x_{t-1},y_{t-1})], \tag{3a}$$

$$y_t=(\mathbf{C}+l\mathbf{I})^{-1}[ly_{t-1}-w_{\text{image}}f_{\text{img\_}y}(\mathbf{x}_{t-1},\mathbf{y}_{t-1})+w_{\text{adpt}}f_{\text{adpt\_}y}(x_{t-1},y_{t-1})], \tag{3b}$$

where $f_{\text{img\_}x}=\partial E_{\text{image}}(x,y)/\partial x_{t-1}$ and $f_{\text{img\_}y}(i)=\partial E_{\text{image}}(x,y)/\partial y_{t-1}$ are image forces, $f_{\text{adpt\_}x}$ and $f_{\text{adpt\_}y}$ are adaptive external forces, l is a step size, $\mathbf{I}$ is a unit matrix, x_t is the x coordinate of the contour node at the current time t, x_{t-1} is the x coordinate at the last time $t-1$, and $\mathbf{C}$ is a pentadiagonal matrix that includes the shape weighting coefficients $\alpha(s)$ and $\beta(s)$. Considering that the derivative of the external forces requires changing $\mathbf{C}$ at each iterative, so we achieve faster iteration by simply assuming the external forces constant during a time step.

Equations (3) are different from the conventional snakes. Here, two items, a multigradient field image force and an adaptive expanding force, are introduced for the purpose of multilayer boundary detection. We use Eqs. (3) to explain the multigradient field concept and show how to apply multigradient field force and adaptive expanding force in our active contour on different phase of the multiple-layer detection.

2.3 *Adaptive Expanding Force*

The expanding force is used to make the contour deform across the homogeneous region of image. The adaptive characteristic adaptively decreases the value of the force when the active contour detects an increase of the gradient field. Subsequent decrease of the adaptive force reduce the step of further expansion and avoid running over the edge. This also reduces the moving steps of those segments on the contour that are located in a homogenous area. The adaptive force is defined by,

$$f_{\text{adpt}}(\mathbf{v}(s))=\frac{1}{\{\sum_{i=1}^{n}|\nabla\mathbf{I}[x(i),y(i)]|\}/n+T}, \tag{4}$$

where n is number of nodes on the active contour, and T is a threshold to keep the force bounded while the sum of gradient is near to zero. This means the adaptive force is an inverse value of the sum of gradient magnitudes in the image where the active contour locates. An adaptive expanding force has a flexible use in different phase of deformation of the contour during the boundary detection. A more detailed explanation of its practical use is given in the following section.

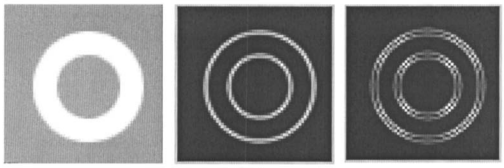

(a) Original image (b) First-order gradient image (c) Second-order gradient image

(Note: Because the image is 60 × 60 pixels in size, it is a normal phenomenon with jagged edges (one square is one pixel) when it is enlarged and displayed here).

Fig. 2 Comparison of first-order gradient image and second-order gradient image.

2.4 *Multigradient Vector Field*

Our original idea is to detect the rectal muscular layers one by one from inner to outer by an unique active contour, which is initially placed at the balloon region. When one boundary of a layer is detected, the algorithm should be able to drive the active contour to expand again and search the outer boundary of the layer automatically. The traditional snakes algorithm cannot meet this requirement, because after finding a boundary it has arrived at an energy minimum and cannot deform again. That is the intrinsic feature of the snakes method.

According to our requirement, after an active contour has extracted the inner boundary of the first layer and gone into the phase of the outer boundary searching of the same layer, it would be best if the current image constraints for the active contour could vanish. This would enable the active model to expand again and search for the next energy minimum. One straightforward idea is to increase the expanding force until it is greater than the synthetic forces from the combination of internal force and current image force; thus, this external force can cause this contour to escape from the current local minimal energy constraints. This, however, is not an optimal method, because relying on this kind of external force would run a risk that the whole model would become more unstable and uncontrollable. A possible result is that the contour may run over the next boundary. The adaptive expanding force is only tailored to undertake the contour's expanding task in the homogenous region in our algorithm.

By analyzing the energy function and kinetic function of traditional snakes, from Eqs. (2a) and (2b), we can find that image energy is a gradient vector field after performing a gradient operation on the original image. The image force, which drives the deformation of the active contour, is a gradient vector field obtained from the gradient operation on the image energy component. It means that image force is a second-order derivative component derived from the original image.

To explain the multigradient field algorithm, two gradient vector fields are defined to clarify the purpose. Here, a ring-shaped image [a white ring on a black background (Fig. 2(a))] is used as an example to illustrate these two

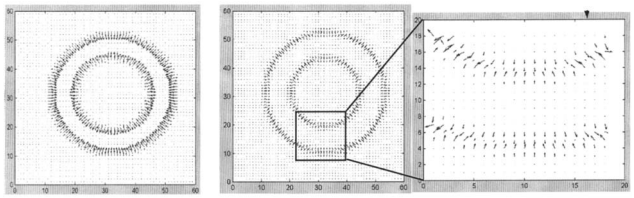

(a) Gradient vector field based on original image – first-order gradient vector field

(b) Gradient vector field based on gradient image–second-order gradient vector field and its enlarged part

Fig. 3 FOGVF and SOGVF.

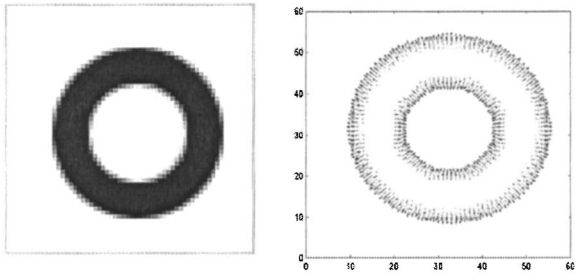

(a) Inverse map of the original image

(b) First-order gradient field of the inverse map

Fig. 4 Inverse map of the original image (Fig. 2(a)) and its first-order gradient field.

concepts:

1. *First-order gradient vector field* (FOGVF): Gradient vector field obtained from the gradient operation on an original image. The corresponding image is called the first-order gradient image (map) $I_{\mathrm{FOGM}}(i,j)$, as shown in Fig. 2(b).
2. *Second-order gradient vector field* (SOGVF): Gradient vector field obtained from the gradient operation on the first-order gradient map. The corresponding image is called second-order gradient image (map) $I_{\mathrm{SOGM}}(i,j)$ [Fig. 2(c)].

Figure 3 shows these two corresponding gradient vector fields. From Fig. 3(b), it is found that the edge of the ring is constrained by two opposite gradient vector fields—centripetal vectors and centrifugal vectors, which are actually the characteristics from the second-order gradient field. On one hand, just these two vector fields, which act as image forces, constrain the active contour's deformation. Under these constraints, the active contour can find the edge of the object when arriving at the minimum energy. On the other hand, if the centripetal force exists, it is just the force that prevents this active contour from expanding and deforming again. Thus, on the second-order gradient field, we cannot hope to use the gradient force to help the contour escape from its current energy minimum.

However, through viewing the first-order gradient field [Fig. 3(a)], we can find that the centripetal gradient vectors in the inner boundary disappear because of the features of the first-order gradient field that gradient vectors always point from low gray level to high gray level on the object's boundary. The exiting centrifugal gradient field is exactly the image force we require that can be used to push the active contour expand and escape from the gravity of the inner boundary. One important point is that the orientation of the first-order-gradient vector will be totally different when we face an inverse image with a black ring on a white background [Fig. 4(a)]. From Fig. 4(b), we can find that the orientation of the gradient vector on the inner boundary is centripetal. For this kind of situation, we should use a different gradient field as the image force, which is obtained not from the original image but from the inverse map of the original image. Here, the inverse map of the image means whose gray values are assigned their mirror transparency. On an inverse map of the original image, the orientation of the gradient vectors on the inner boundary becomes centrifugal, just like those on the image with a white ring on a black background. Therefore, knowledge about the image structure should be known before using a suitable gradient field.

Based on the preceding analysis, we developed a novel active contour model incorporating multigradient vector field (multi-GVF) algorithm. This model, which we called the multigradient field active contour model, can complete multilayer boundary detection. Figure 5 shows how to detect the inner boundary and outer boundary of a ring. Here, we adopt the image with black ring on white background as an example. The detailed procedure of an algorithm implementation is described as follows:

1. Compute the FOGVF and SOGVF of the original image, and the FOGVF of the inverse image.
2. Set up the initial active contour (a circle) in the central region of the ring. The initial contour should be fully encircled by the ring.
3. Deform the active contour under the constraint of the internal forces, image forces and expanding forces. The corresponding numerical functions are

$$x_t = (\mathbf{C} + l\mathbf{I})^{-1}\{[lx_{t-1} - w_{\mathrm{image}}\partial E_{\mathrm{image}}(x_{t-1},y_{t-1})]/\partial x_{t-1} + w_{\mathrm{adpt}} f_{\mathrm{adpt}\_x}(x_{t-1},y_{t-1})\}, \tag{5a}$$

$$y_t = (\mathbf{C} + l\mathbf{I})^{-1}\{[ly_{t-1} - w_{\mathrm{image}}\partial E_{\mathrm{image}}(x_{t-1},y_{t-1})]/\partial y_{t-1} + w_{\mathrm{adpt}} f_{\mathrm{adpt}\_y}(x_{t-1},y_{t-1})\}. \tag{5b}$$

   Here, the two terms of image force are the second-order gradient fields: $\partial E_{\mathrm{image}}(x_{t-1},y_{t-1})/\partial x_{t-1}$ and $\partial E_{\mathrm{image}}(x_{t-1},y_{t-1})/\partial y_{t-1}$. The adaptive expanding forces in Eq. (4) are used here. In the homogenous region, the adaptive expending forces play an important role to deform the active contour. In the capture range of the boundary, the adaptive expanding forces decrease, and the image forces (SOGVF) act as strong constraints on the deformation of the contour. When this active contour reaches the equilibrium of its energy, the inner boundary of the ring is detected. Because the image forces are zero, the expanding forces also reach their minimum.
4. Use the preceding resulting contour as a new initial one and deform the active contour model again under

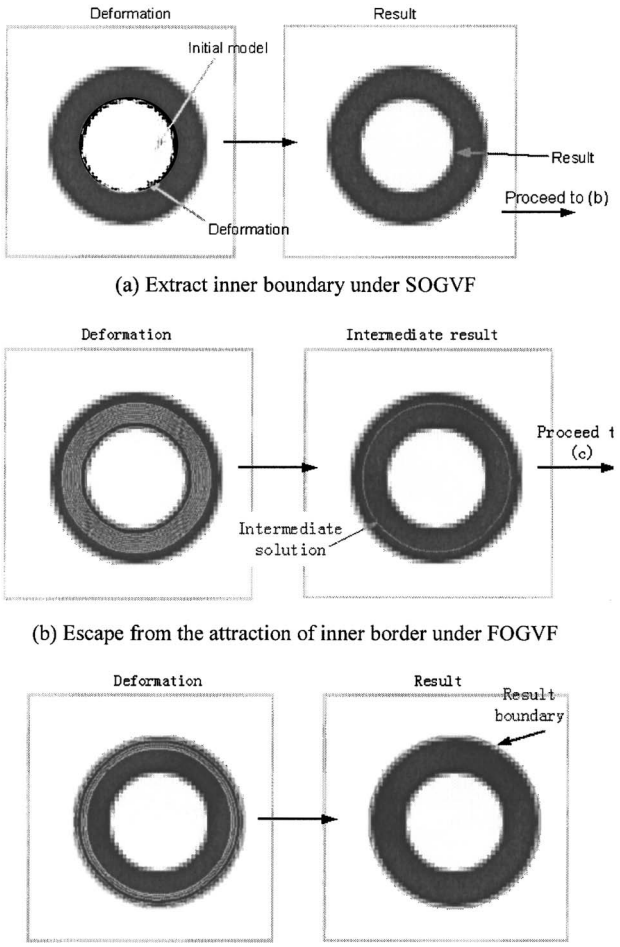

Fig. 5 Inner border and outer border detection by two different GVFs as the image force.

the constraints of the internal forces, image forces, and expanding forces. The corresponding numerical equations become

$$x_t = (\mathbf{C} + l\mathbf{I})^{-1}[lx_{t-1} - w_{\text{image}}E_{\text{image\_}x}(x_{t-1}, y_{t-1}) + w_{\text{adpt}}f_{\text{adpt\_}x}(x_{t-1}, y_{t-1})], \tag{6a}$$

$$y_t = (\mathbf{C} + l\mathbf{I})^{-1}[ly_{t-1} - w_{\text{image}}E_{\text{image\_}y}(x_{t-1}, y_{t-1}) + w_{\text{adpt}}f_{\text{adpt\_}y}(x_{t-1}, y_{t-1})]. \tag{6b}$$

In the current process, the image forces are the first-order gradient vectors derived from the inverse map of the original image. The expanding forces are chosen as a constant rather than as an adaptive one. Because the image is a black ring on a white background, the orientation of FOGVF from inverse image is centrifugal on the inner boundary as what we wish. This centrifugal image and expanding force can help active contour escape from the current location, as illustrated in Fig. 5(b). The active contour passes across the homogeneous area of the ring and finally reaches the equilibrium of its energy when it is near to the outer boundary of the ring. The current equilibrium can also be explained as a kind of force equilibrium between the internal forces, centrifugal expanding forces and centripetal image forces (FOGVF on the outer boundary of the ring). Here, expanding forces and image forces are two opposing forces. Because the equilibrium location is not the minimum of the second-order image force, the current location is not really a place of the outer boundary, just near to it, as shown in Fig. 5(c).

5. This step is a fine-tuning or refinement of the outer boundary finding. The SOGVF is used again as in step 3, and the contour model continues to deform under the second-order gradient vectors, internal forces, and adaptive expanding forces. Finally, when energy minimum of the contour is reached, the accurate location of the outer boundary is obtained [Fig. 5(c)].

If there are more concentric layers outside, the algorithm can repeat steps 3 and 4 and complete the detection of each layer, but the image force should be treated carefully. For example, if there is another layer outside, we require a centrifugal image force again as image force. To meet this requirement, at this time, FOGVF should be calculated from the original image. Thus, there is a simple regulation for this kind of concentric layer structure's detection. If the detecting procedure is from inner to outer, first we should judge the FOGVF orientation of the innermost boundary, then choose the FOGVF for a different boundary alternatively from the original image or the inverse map of the original image.

3 Experimental Results

In this section, the algorithm was first applied on a synthetic image as well as a simulated ultrasound image for boundary finding. The implementation of the algorithm on these images and their corresponding results represents some general features of the model. Next, the algorithm was applied for rectal wall boundary detection and anal wall boundary detection. Some specific settings and approaches given in the processing procedure on these two kinds of image showed the flexibility and speciality of the algorithm for different purpose of boundary detection on different objects. Finally, we assessed the algorithm on rectal wall ultrasound images and evaluated if it is acceptable by clinical experts.

3.1 *Applying the Algorithm on Synthetic and Simulated Ultrasound Images*

Figure 6 shows the results of applying multigradient field active contour model for boundary finding on a noisy synthetic image. The image can be considered as a structure of multiple ring-shaped objects, which enclose. The average gray value of all "white" regions is 192, and that of all "black" regions 128. The standard deviation of the noise is 68. It is very clear that the low-level threshold method is not suitable for boundary detection because the standard deviation of the noise is greater than the difference of gray values between two regions.

The original image is first blurred by a Gaussian filter. Then, its boundaries are detected using a multigradient

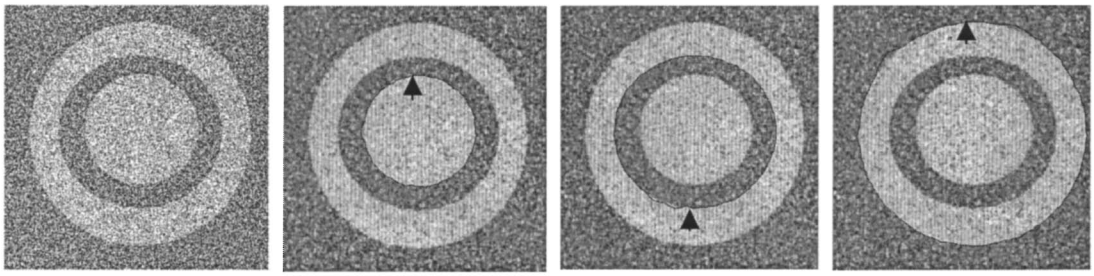

(a) (b) (c) (d)

(Note: Synthetic image generated by computer, with high noise level. Image size is 372 × 371 . (a)–(d) show the resulting boundaries, which are detected from inner to outer by multigradient field active contour algorithm. (a) is original image. (b) - (d) are filtered by Gaussian smoothing.)

Fig. 6 Test on synthetic image.

field-active contour. The initial contour model is placed in the central area of the image. The procedure of boundary detection is implemented from inner to outer. It is shown that active contour has settled itself on the energy minimum at each detection phase and three boundaries are detected accurately.

To evaluate a simulated ultrasound image, we adopted the freeware software Field II (Ref. 37), as the ultrasound simulation software, which is developed by Professor JØrgen Arendt Jensen of Denmark University. Field II is a set of programs for simulating ultrasound transducer fields and ultrasound imaging using linear acoustics. The programs use the Tupholme-Stepanishen method for calculating pulsed ultrasound fields. Because Field II supplies only the necessary routines for implementing the simulation of the various ultrasound transducers, users should set up their own application software.

Based on the routines supplied by Field II, we developed our own programs for rectal wall ultrasound imaging simulation. The whole process is first to generate an artificial phantom by drawing a bitmap image with scattering strength of the region of interest. Then the programming work is needed, involving scatterers image generation subroutine, transducer simulation subroutine, field simulation and data creation subroutine, and the final image creation subroutine. The final step is to run the programs and obtain the simulated ultrasound image. Due to the complexity of the algorithm and the large amount of data that must be processed, the time to create an ultrasound image is near to 5 to 7 days on a Pentium II 300 MHz computer.

Figures7(a) and 7(b) illustrate two-boundary detection results on two simulated ultrasound images, the former has clearer boundaries than the latter. The white curves represent the boundaries detected by the algorithm according to the same approach that detects the boundaries from inner to outer layer by layer. From the result, it is found the boundaries were detected successfully.

3.2 *Multilayer Boundary Detection of the Rectal Wall and Anal Wall*

The pictures given in Fig. 8 illustrate the deformation process of the multigradient field active contour and the corresponding detection results of the rectal muscular layer boundaries by using multigradient field active contour algorithm. According to the algorithm, three different gradient vector fields and their corresponding gradient maps are created and used as image forces at different detection phases. These include

1. FOGVF and first-order gradient map of the original image
2. SOGVF and second-order gradient map of the original image
3. FOGVF and first-order gradient map of the inverse image

Figure 8(a) shows the process of the innermost boundary detection on a rectal wall image. The initial active contour is set as a circle and placed in the balloon area. Because of the features of the active contour model, ultrasound probe (indicated by white arrow) should be at the interior of the contour. A series of expanding contours shown on the image represent the boundary searching in progress. Figure 8(b) gives obtained inner boundary of the first muscular layer (lamina propria layer). From it, we can find that a good result of the innermost boundary is obtained because of the relatively good edge features of the boundary. The adaptive forces derived from $w_{\mathrm{adp}}E_{\mathrm{adpt}}$ actually supply a more flexible and stable control for the expanding process of the active contour.

Figures 8(c)–8(e) show two phases using active contour to find the outer boundary of the first muscular layer. Two different gradient fields—the FOGVF and the SOGVF—

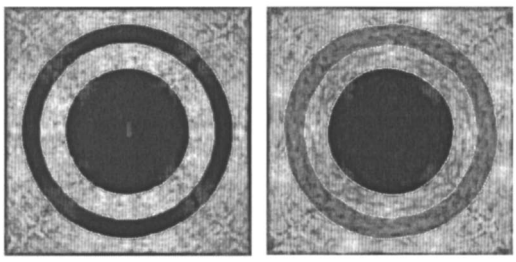

(a) (b)

Fig. 7 Boundary detection on two simulated phantoms (white lines represent the detected boundaries).

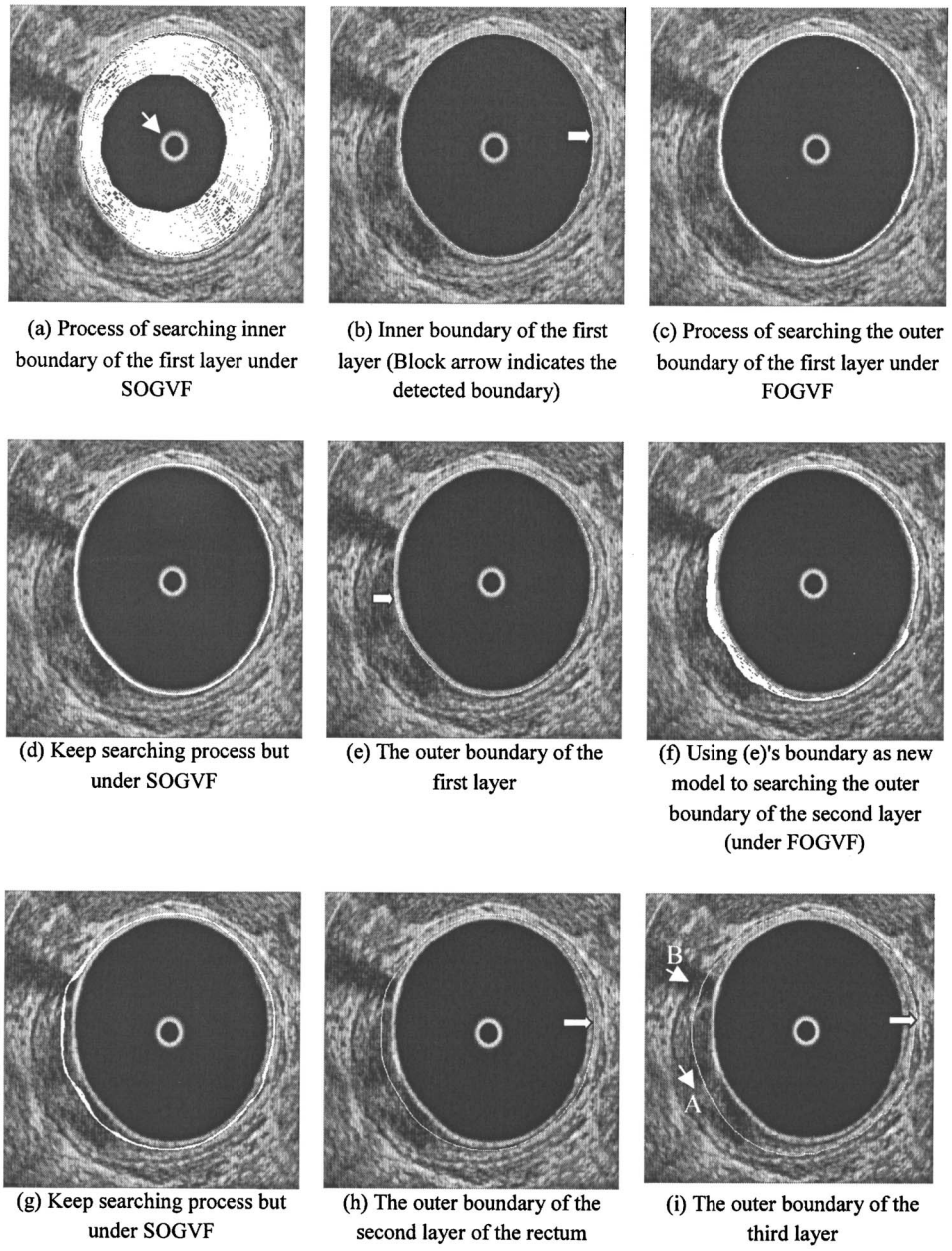

Fig. 8 Detecting the three-layer boundary of the rectum.

are used as image forces to control the deformation of the contour at two different phases. At the first phase, the FOGVF from original image, which can help active contour escape from the capture range of the inner boundary, controls the deformation of the active contour [Fig. 8(c)]. Internal force helps constrain the shape of contour, and expanding force helps contour pass across the homogeneous region. An intermediate result is obtained at the first phase. This temporary contour locates in the middle between the inner boundary and the outer boundary of the first layer but more close to the outer boundary. At the second phase, active contour deforms under SOGVF and goes on the process of finding outer boundary [Fig. 8(d)]. Figure 8(e) shows the obtained outer boundary of the first muscular layer.

The current obtained boundary can also be considered as the inner boundary of the second layer. As such, we can use this boundary as an initial active contour and start the next searching process. Note, however, that the image forces that drive the contour's expansion are from the FOGVF of the inverse image rather that from that of the original image. This is because we must keep the image forces as centrifugal forces that have the ability to drive the contour outward and escape from the current position. If we use the FOGVF from original image, the image forces will be centripetal ones, which will drive the contour inward to the area of the first layer [the gradient field in Fig. 3(a) illustrates this principle]. The following steps are the same as the two phases already mentioned. Figures 8(f) and 8(g) show two phases of the outer boundary finding of the sec-

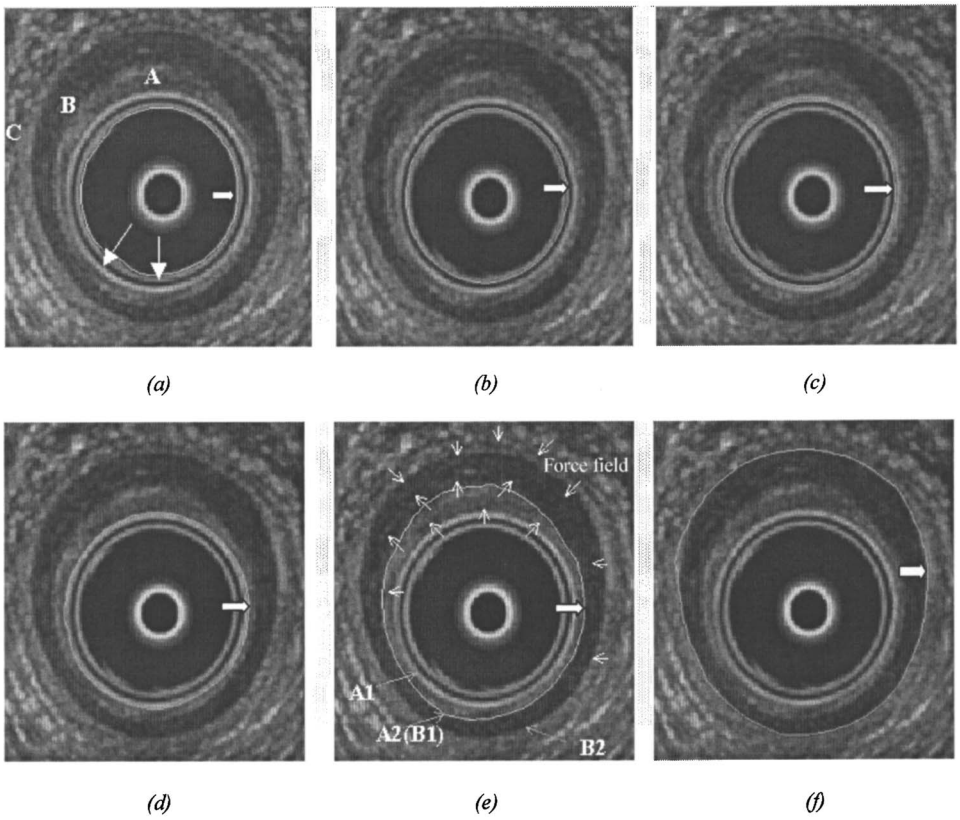

(Note: Image size is 300 × 340 . Inner two bright interfaces are from the plastic cap. (a)-(c) Detected boundaries of the cone. (d) Inner boundary of the subepithelial tissues. (e) Outer boundary of the subepithelial tissues, which is also the inner boundary of the internal anal sphincter. (f) Outer boundary of the internal anal sphincter. Block arrow indicates the boundary.)

Fig. 9 Boundary detection on an anal wall ultrasound image.

ond muscular layer. Figure 8(h) shows the obtained boundary. Through the similar process, the outer boundary of the third layer can be found [Fig. 8(i)].

The features existing in the preceding results can be concluded about as follows. Although the second layer is very thin, it is found that the new algorithm can distinguish and extract its boundary. Benefiting from its closed contour feature, active contour can keep the pseudocontours on the broken regions of the muscular layers like in tumor region A (white arrows) and artifact region B (white arrow).

In the following case, the multigradient field active contour algorithm is used for boundary finding (block arrow indicating the detected boundary) on a cross-sectional ultrasound image of anal canal (Fig. 9). It is shown the proposed multigradient field algorithm has the ability to cope with the multiboundary detection issue of other targets such as the anal canal, which have a concentric muscular layer structure similar to rectal wall. Figure 9(a) illustrates the cross-sectional structure of the anal canal on an ultrasound image. There are two bright interfaces from the probe cone (white arrows). Region A is a muscular layer from the moderately reflective subepithelial tissue. Region B represents the poorly reflective internal anal sphincter. Region C indicates the longitudinal internal muscle. External anal sphincter out of layer C is not shown in the image. An initial active contour is placed at the central black area. The method of boundary detection of the cone shown in Figs. 9(a)–9(d) is similar to the preceding two examples. The FOGVF of original image and the FOGVF of inverse image are used alternately to drive active contour escape from the current constraints and expand outwards. SOGVF is used to make the contour converge to the energy minimum. But for boundary finding of the outer boundary (A2) of layer A and outer boundary (B2) of layer B, there is a tricky method for using FOGVF, shown in Figs. 9(e) and 9(f). When the active contour escapes from the inner boundary (A1) of layer A for next step searching, FOGVF of inverse image is used as images forces. As shown in Fig. 9(e), the image forces of inverse image point outwards at both A1 and A2, because of the ultrasound features of subepithelial tissue (layer A) and internal anal sphincter (layer B). Therefore, the active contour will not stop when near to A2. It will expand continuously under FOGVF and stop at the equilibrium position near to B2. Then, under SOGVF, the contour can find the outer boundary of layer B. For finding A2, the contour of B2 is used as the initial one. Adaptive expanding forces should be converted to shrinking forces by simply changing their signs in the numerical equation. At this time, the contour deforms under the shrinking force and FOGVF of inverse image. It will shrink and stop at the equilibrium location near to A2. Then under SOGVF, the contour can converge to the outer boundary of layer A.

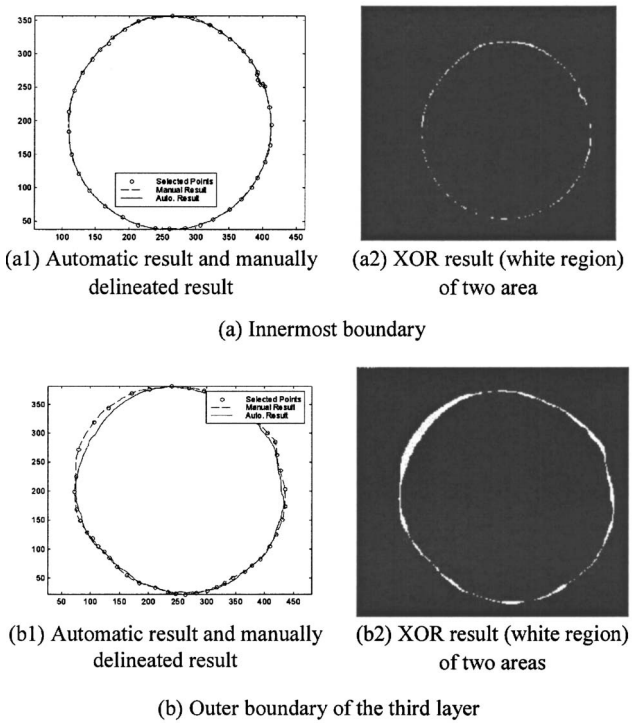

Fig. 10 Comparison of automatic results with manual results.

From this example, we can conclude that for different organs with different layer structures, we should have the *a priori* knowledge about the feature of the structure. Then this knowledge can be integrated into the algorithm and help to determine how to apply different FOGVFs at different detecting phases.

3.3 *Assessment of the Algorithm*

Figure 10 illustrates the results of automatic detection and one of manual delineations on the image shown in Fig. 8 (image 1 in Table 1). For the reason of convenient observation, we do not draw them on source image but draw them separately. It is found that the detecting result of the innermost boundary is very good. The detecting result for the third layer's outer boundary is also good.

Figure 11 shows another result from image 3. It also has a good result. The difference between automatic result and manual result is mainly on the tumor region. In this part, the contour obtained by automatic algorithm has a little bit of shrinkage because of the effect of the internal force. It is also found that some boundaries at the top of the rectal wall are cohesive together or one layer's boundary jumps to another layer. Carefully viewing the result and analyzing the gradient in these parts, we found it is a reasonable result because on these parts the gradient fields are weak or none (two layers merge into one) and even surgeons cannot confirm the real position of the boundary from an ultrasound image. Therefore, it is hard to distinguish the boundaries by the current algorithm. A suggestion is that more prior knowledge about the rectal structure and interaction from

Table 1 Computer expert difference versus interexpert difference.

Image No.	Expert	IED (pixel unit)	CED	MACED –MAIED
1	E1	(E1–E2) 0.95	0.65	–0.05
	E2	(E2–E3) 0.89	0.90	
	E3	(E3–E1) 0.74	0.75	
2	E1	(E1–E2) 0.91	0.71	–0.08
	E2	(E2–E3) 0.98	0.91	
	E3	(E3–E1) 0.68	0.76	
3	E1	(E1–E2) 1.11	0.95	–0.16
	E2	(E2–E3) 0.71	0.65	
	E3	(E3–E1) 0.98	0.88	
4	E1	(E1–E2) 1.46	1.30	–0.16
	E2	(E2–E3) 0.78	1.01	
	E3	(E3–E1) 1.35	0.66	
5	E1	(E1–E2) 0.91	0.79	–0.12
	E2	(E2–E3) 0.64	0.58	
	E3	(E3–E1) 0.68	0.63	
6	E1	(E1–E2) 0.73	0.91	0.05
	E2	(E2–E3) 0.61	0.64	
	E3	(E3–E1) 0.86	0.88	
7	E1	(E1–E2) 1.38	1.21	–0.17
	E2	(E2–E3) 0.86	0.82	
	E3	(E3–E1) 1.31	1.11	
8	E1	(E1–E2) 1.11	0.82	–0.01
	E2	(E2–E3) 1.01	0.85	
	E3	(E3–E1) 1.21	1.20	
9	E1	(E1–E2) 1.44	1.38	–0.06
	E2	(E2–E3) 0.88	0.69	
	E3	(E3–E1) 1.31	0.68	
10	E1	(E1–E2) 0.74	1.38	0.40
	E2	(E2–E3) 0.88	0.96	
	E3	(E3–E1) 0.98	0.86	

CED, interexpert difference; IED, computer-expert difference; MACED, maximum computer expert distance; MAIED, maximum interexperts distance.

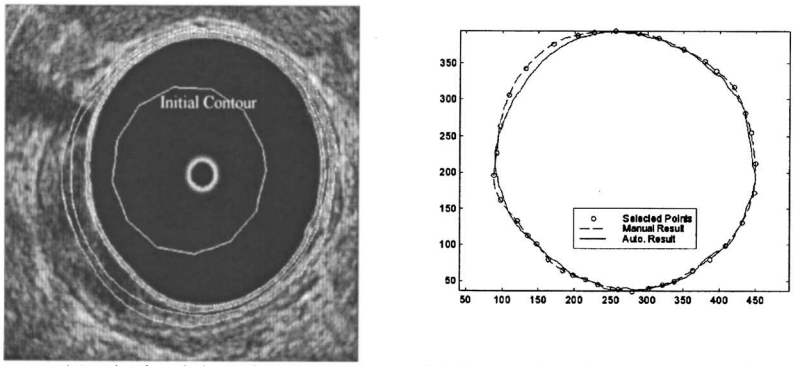

(a) Obtained three layers' boundaries

(b) Comparison between manual result and automatic result for the outer boundary of the third layer

(Note: The image coordinates are different from Cartesian coordinates. The origin of the image coordinates is at top left corner).

Fig. 11 One image and its detection result.

the user should be integrated into the algorithm in the future.

Figure 12 shows a result for image 6. Observing the image, we can find that the image quality on the left-bottom region below the water balloon is very poor. The muscular layer features are hard to find in this area. Thus, our model just can find a subjective boundary of one layer. Therefore, the main difference between automatically detected contour and manually delineated boundary is large in this area, as shown in Fig. 12(b).

To evaluate the algorithm on clinical images, three experts were invited to outline the boundary of desired layer. The experts' outlined results are compared with the computer-detected results. The compared results show the detecting result of the innermost boundary and outer boundary of the first layer are perfect and fully acceptable by three experts. For the rest, because of the obvious difference from the first layer's boundaries, we choose the outer boundary of the third muscular layer as evaluated sample for quantitative analysis. We partially adopt the evaluating equations defined in Ref. 38 to evaluate the performance of the algorithm. The evaluation method can be described briefly as follows.

The mean absolute distance (MEAD) between two curves $\mathcal{A}=\{a_1,a_2,\ldots,a_n\}$ and $\mathcal{B}=\{b_1,b_2,\ldots,b_n\}$ is defined as:

$$e(\mathcal{A},\mathcal{B})=\frac{1}{2}\left[\frac{1}{n}\sum_{i=1}^{n}\mathrm{d}(a_i,\mathcal{B})+\frac{1}{n}\sum_{i=1}^{n}\mathrm{d}(b_i,\mathcal{A})\right], \tag{7}$$

where $\mathrm{d}(a_i,\mathcal{B})=\min_j\|b_j-a_i\|$, called closest distance of point a_i to curve $\mathcal{B}$. MEAD is a general definition and will be replaced in the following by CED (interexpert difference) and IED (computer to expert difference), in particular, representing the mean absolute distance between experts and that between computer and expert, respectively.

The curves outlined by three experts on an image are denoted by $\mathcal{E}_1$, $\mathcal{E}_2$, and $\mathcal{E}_3$. Computer-detected one is denoted by $\mathcal{C}$. Several parameters, used for the validation, is defined as following:

1. Maximum computer-expert distance (MACED) $=\max\{\mathrm{CED}\}=\max\{e(\mathcal{C},\mathcal{E}_1),e(\mathcal{C},\mathcal{E}_2),e(\mathcal{C},\mathcal{E}_3)\}$.
2. Maximum interexperts distance (MAIED) $=\max\{\mathrm{IED}\}=\max\{e(\mathcal{E}_1,\mathcal{E}_2),e(\mathcal{E}_1,\mathcal{E}_3),e(\mathcal{E}_2,\mathcal{E}_3)\}$.

This method, in fact, calculates the difference of expert-delineated results and the difference between computer-detected results and experts' results. Therefore, the method can show the interexpert variability and computer to expert difference at the same time. The synthetic indicator "MACED minus MAIED" represent the acceptable level of computer-detected results by experts.

Table 1 shows the interexpert difference and computer to expert difference for desired boundary detection on 10 rectal wall images. Pixel distance is used as the unit. From the table, it is shown the IED and CED are all not large, showing a good delineated and detecting results. Small IED values represent that the experts agreed with each other on the majority of outlined results. The large IED values represent that there are disagreements between three experts on recognizing the boundaries of some muscle layers.

The last two columns in Table 1 list the computer to expert distance and the difference between maximum computer to expert distance and maximum interexpert distance. We choose difference of MACED and MAIED as our evaluating parameter. If this value is less than zero, it represents the computer-detected result is located in the scope of experts' agreement and more acceptable.

From Table 1, 8 of 10 automatic tracking results are less than zero, thereby being consistent with the experts' results. There are two values greater than zero, representing they are out of the scope formed by three experts. One of these two values are very small, 0.05, representing the tracking results are very near to the experts' outlined results. The last one is larger, therefore representing the result is out of the scope that experts can accept.

4 Conclusions and Discussion

The investigation of rectal wall multilayer delineation on ultrasound images was motivated by the need from clinics

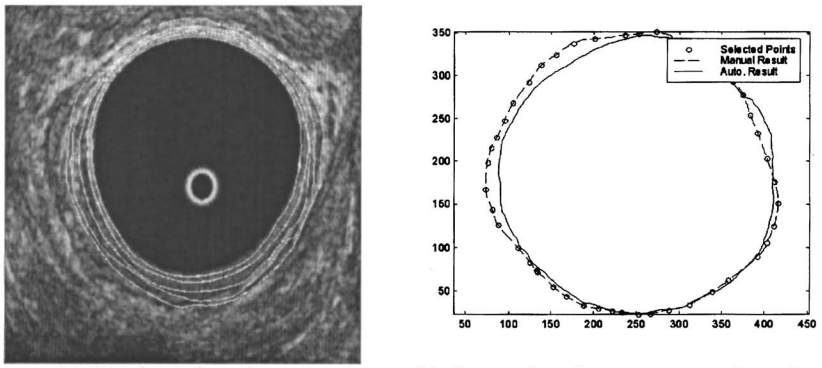

(a) Obtained three layers' boundaries

(b) Comparison between manual result and automatic result for the outer boundary of the third layer

(Note: The image coordinates are different from Cartesian coordinates. The origin of the image coordinates is at top left corner).

Fig. 12 One image with partially poor quality and its boundary-finding results.

for a 3-D structure of rectum detection from ultrasound images that is helpful for clinical diagnosis. Current ultrasound imaging systems provide only some basic display functions for 2-D image and 3-D volume views as well as some corresponding basic measure functions for distance and circumference measure, etc. However, a 3-D surface rendering constructed by detected boundaries of rectal muscle layers and a suspicious tumor from the ultrasound images would be a more intuitive visualization in front of a surgeon. For example, the 3-D visualization of rectum can directly present how many layers are penetrated by a suspicious tumor. This is important for rectal tumor staging. Further, some basic functions, such as calculating suspicious tumor volume or measuring the length of a broken layer, can be easily implemented based on the coordinate information of the detected boundaries. More quantitative rather qualitative parameters can be given by the system. All these are a grand goal. Therefore, the boundary detection of rectal wall layers[35] and suspicious tumor[39] is the crucial step of the goal. This paper presents only the first-stage work involving rectal wall boundary detection.

Boundary detection of the rectal muscular layers is difficult because of the low spatial resolution of ultrasound images, the thinness of the rectal layer, and the absence of the layer segment penetrated by the tumor. Therefore, conventional approaches, such as low-level edge detection and the edge-linking method, did not meet the study's requirement. Some other high-level methods also have their limitations for the requirement of multilayer detection of the rectal structure.

The active contour model, snakes, has been used by many researchers for boundary detection in image processing. With the snakes method, anatomical knowledge of the rectum can be integrated into layer-detecting procedures. One of the limitations of the snakes method is its requirement that the initial contour to be placed near the desired edge of the object and its ability to perform only single object recognition. Therefore, for this study, the tradition snakes method was not capable of implementing multilayer boundary detection of the rectal wall.

The multigradient field active contour model proposed in this paper solved this limitation when applied for rectal muscular layer's boundary detection. In the paper, the FOGVFs and SOGVFs were illustrated. Based on them, a novel multigradient vector field algorithm was proposed and introduced into the active contour model. This algorithm makes the active contour able to escape the trammel from the present layer and go on the next layer searching and finally realize the multilayer detection successfully. Adaptive force, which can produce compensation between internal force and image force, especially in homogeneous regions in an image, also plays an important role in the practical application. Some general features such as convergence and the stability of the model are not discussed here, because these features are not different between the multigradient field model and the traditional model.

Several problems should be considered in future. For a normal rectal wall without disease, the real boundary for each layer can be delineated correctly. But for cases in which some muscular layers are penetrated by tumor, this algorithm just gives a closed contour for each boundary because of the features of active contour model [Fig. 8(f)]. Thus, a further work on how to distinguish the real boundary from the virtual boundary that is the tumor part should be done. Another problem is that during the process of deformation, the active contour sometimes is easily attracted by some "isolated islands" and forms an irregular border. The reason is due to the irregularity of the boundary and some small broken segments on the layer.

Preprocessing the image may be able to solve these defects inherent in ultrasound images. In this paper, we emphasize the general features of the algorithm, so no *a priori* knowledge about rectal anatomical structure was incorporated into the algorithm. To set up a more accurate model for rectal wall layer detection, more prior knowledge and constraints should be incorporated into the basic model.

The current algorithm was programmed based on the MATLAB language and evaluated on several cases for research purpose. To reach clinical applicability, a good interface and interactive system based in the C++ language

should be developed. Based on this system, then, a large-scale clinical test should be performed in future work for different cases.

References

1. A. R. Wojtowycz, "Endoscopic US of the gastrointestinal tract with endoscopic, radiographic, and pathologic correlation," *Radiographics* **15**(4), 735–753 (1995).
2. A. A. Yong and S. A. Roberts, "Interventional endoscopic ultrasound," *Clin. Radiol.* **58**(1), 32–43 (2003).
3. J. W. Fleshman, H. Nelson, and W. R. Peters, "Early results of laparoscopic surgery for colorectal cancer: retrospective analysis of 372 patients treated by Clinical Outcomes of Surgical Therapy (COST) Study Group," *Dis. Colon Rectum* **39**(10, Supp.), S53–S58 (1996).
4. M. J. Wiersema and G. C. Harewood, "Endoscopic ultrasound for rectal cancer," *Gastroenterol. Clin. North Am.* **31**(4), 1093–105 (2002).
5. D. F. Ransohoff and C. A. Lang, "Screening for colorectal cancer," *N. Engl. J. Med.* **325**(1), 37–41 (1991).
6. A. Kumar and J. H. Scholefield, "Endosonography of the anal canal and rectum," *World J. Surg.* **24**(2), 208–215 (2000).
7. Y. Saitoh, T. Obara, K. Einami, M. Nomura, M. Taruishi, T. Ayabe, T. Ashida, Y. Shibata, and Y. Kohgo, "Efficacy of high-frequency ultrasound probes for the preoperative staging of invasion depth in flat and depressed colorectal tumors," *Gastrointest Endosc* **44**(1), 34–39 (1996).
8. M. Brejl and M. Sonka, "Medical image segmentation: automated design of border detection criteria from examples," *J. Electron. Imaging* **8**, 54–64 (1999).
9. M. Sonka and X. Zhang, "Segmentation of intravascular ultrasound images: a knowledge-based approach," *IEEE Trans. Med. Imaging* **14**, 719–732 (1995).
10. M. Kass, A. Witkin, and D. Terzopoulos, "Snake active contour model," *Int. J. Comput. Vis.* **1**, 321–331 (1987).
11. A. A. Amini, S. Tehrani, and T. E. Weymouth, "Using dynamic programming for minimising the energy of active contours in the presence of hard constraints," in *Proc. 2nd Int. Conf. on Computer Vision*, pp. 95–99, Tarpon Springs (1988).
12. D. J. Williams and M. Shah, "A fast algorithm for active contours," in *Proc. 3rd Int. Conf. on Computer Vision*, ISBN: 0–8186–2057–9, pp. 592–595 (1990).
13. S. Menet, P. Saint-Marc, and G. Medioni, "B-snakes: Implementation and application to stereo," in DARPA Image Understanding Workshop, pp. 720–726, Pittsburgh (1990).
14. P. Brigger, J. Hoeg, and M. Unser, "B-spline snakes: a flexible tool for parametric contour detection," *IEEE Trans. Image Process.* **9**(9), 1484–1496 (2000).
15. L. D. Cohen, "On active contour models and balloons," *CVGIP: Image Understand.* **53**(2), 211–218 (1991).
16. L. D. Cohen and I. Cohen, "A finite element method applied to new active contour models and 3D reconstruction from cross sections," in *Proc. 3rd Int. Conf. on Computer Vision*, pp. 587–591, IEEE Computer Soc. Press (1990).
17. G. Xu and E. Segawa, "A robust contour model with insensitive parameters," in *Proc., 4th Int. Conf. on Computer Vision*, ISBN: 0–8186–3870–2, pp. 562–566 (1993).
18. C. Xu and J. L. Prince, "Snakes, shapes, and gradient vector flow," *IEEE Trans. Image Process.* **7**, 359–369 (1998).
19. C. Xu and J. L. Prince, "Global optimality of gradient vector flow," in *Proc. 34th Annu. Conf. on Information Sciences and Systems (CISS'00)*, pp. 15–17, Princeton University (Mar. 2000).
20. C. Cañero, F. Vilariño, J. Mauri, and P. Radeva, "Predictive (un)distortion model and 3D reconstruction by biplane snakes," *IEEE Trans. Med. Imaging* **21**(9), 1188–1201 (2002).
21. J. Liang, T. McInerney, and D. Terzopoulos, "United snakes," in *Proc. 7th IEEE Int. Conf. on Computer Vision*, Vol. 2, pp. 933–940, IEEE Computer Soc. Press (1999).
22. D. Cheng and A. Schmidt-Trucksass, "Using snakes to detect the intimal and adventitial layers of the common carotid artery wall in the sonographic images," *Comput. Methods Programs Biomed.* **67**, 27–37 (2002).
23. S. H. Matthew, "A statistical active contour model for SAR image segmentation," *Image Vis. Comput.* **17**, 213–224 (1999).
24. X. M. Pardo, P. Radeva, and D. Cabello, "Discriminant snakes for 3D reconstruction of anatomical organs," *Med. Image Anal* **7**(3), 293–310 (2003).
25. L. Ji and H. Yan, "Robust topology-adaptive snakes for image segmentation," *Image Vis. Comput.* **20**(2), 147–164 (2002).
26. A. Chakraborty, L. H. Staib, and J. S. Duncan, "Deformable boundary finding in medical images by integrating gradient and region information," *IEEE Trans. Med. Imaging* **15**, 859–870 (1996).
27. H. Wu and G. Bijoy, "Geometric active deformable models in shape modeling," *IEEE Trans. Image Process.* **9**, 302–308 (2000).
28. J. Park, D. Metaxas, and L. Axel, "Volumetric deformable models with parameter functions: a new approach to the 3D motion analysis of the LV from MRI-SP AMM," in *Proc. 5th Int. Conf. on Computer Vision*, pp. 700–705, IEEE Computer Soc. Press (1995).
29. W. Kim and J. Lee, "Visual tracking using snake for object's discrete motion," in *Proc. IEEE Int. Conf. on Robotics and Automation*, pp. 2608–2613, IEEE Press (2001).
30. H. Park, T. Schoepflin, and Y. Kim, "Active contour model with gradient directional information: directional snake," *IEEE Trans. Circuits Syst. Video Technol.* **11**(2), 252–256 (2001).
31. T. McInerney and D. Terzopoulos, "A dynamic finite element surface model for segmentation and tracking in multidimensional medical images with application to cardiac 4D image analysis," *Comput. Med. Imaging Graph.* **19**(1), 69–83 (1995).
32. R. Szeliski and S. Lavallee, "Matching 3-D anatomical surfaces with non-rigid deformations using octree-splines," *Int. J. Comput. Vis.* **18**(2), 171–186 (1996).
33. M. Moshfeghi, S. Ranganath, and K. Nawyn, "Three-dimensional elastic matching of volumes," *IEEE Trans. Image Process.* **32**, 128–138 (1994).
34. T. McInerney and D. Terzopoulos, "Deformable models in medical image analysis: a survey," *Med. Image Anal* **1**(2), 91–108 (1996).
35. D. Xiao, W. S. Ng, U. R. Abeyratne, C. B. Tsang, and K. C. Kwoh, "Rectal wall structure delineation and broken layer recognition by multigradient field active contour," *Australian and New Zealand Intelligent Information System Conf.*, pp. 124–127, IEEE Press (2001).
36. D. Xiao, W. S. Ng, U. R. Abeyratne, C. B. Tsang, and F. Liu, "Hardware and algorithm design for rectal wall ultrasound image acquisition and analysis," in *Proc. Kuala Lumpur Int. Conf. on Biomedical Engineering*, pp. 106–109, University of Malaysia (2002).
37. J. A. Jensen, "Field: a program for simulating ultrasound systems," *Med. Biol. Eng. Comput.* **34**(Suppl. 1, Part 1), 351–353 (1996).
38. V. Chalana, D. T. Linker, D. R. Haynor, and Y. Kim, "A multiple active contour model for cardiac boundary detection on echocardiographic sequences," *IEEE Trans. Med. Imaging* **15**(3), 290–298 (1996).
39. D. Xiao, W. S. Ng, U. R. Abeyratne, and C. B. Tsang, "Rectal tumor boundary detection by unifying active contour model," in *Medical Imaging, Proc.*, *Proc. SPIE* **4684**, 1415–1426 (2002).

Di Xiao received his BEng degree in biomedical engineering and instruments and his MEng degree in electrical engineering from Chongqing University, China, and his PhD degree from the Nanyang Technological University, Singapore. From 1993 to 1999 he was a lecturer with the Electronic Department at Chongqing University, and was mainly engaged in the research on biomedical signal processing and biomedical instrument design. From 2002 to 2004 he was a research scientist for the prostate needle biopsy robot project at Singapore General Hospital. Dr. Xiao is currently a senior research fellow for the anorectal image processing and reconstruction project with National University Hospital, Singapore. His research interests include biomedical signal processing, biomedical image processing, and medical robotic design.

Wan Sing Ng heads and founded the Computer Integrated Medical Intervention Laboratory at Nanyang Technical University, where he is an associate professor in the School of Mechanical and Production Engineering. He received his BEng and MEng degrees from the National University of Singapore and his PhD degree from Imperial College, London. Ng is a professional engineer (P.Eng Singapore), a chartered engineer, and a fellow of the Institute of Mechanical Engineering, United Kingdom, and a member of the IEEE. His research interests include medical robotics, computer assistance in surgery, and the safety of medical robots. His research aims to help surgeons to do their job better with improved outcomes and productivity and his collaborating partners include those from local hospitals as well as overseas research institutions.

Udantha R. Abeyratne received his BSc (Hons.) degree in electrical and electronic engineering from the University of Peradeniya, Sri Lanka, his MS degree in electrical engineering from the University of Tokushima, Japan, and his PhD degree in biomedical engineering and science from Drexel University, Philadelphia, in 1996. From 1997 to 2002 he was an assistant professor with Nanyang Technological University, Singapore, and since 2002 has been a senior lecturer in biomedical engineering with the University of Queensland, Brisbane, Australia. His research interests include ultrasound imaging, medical instrumentation, and signal processing, with special focus in the area of low-cost technologies for mass-screening. Dr. Abeyratne has earned many accolades for his work, including Monbusho and Calhound Fellowships and several Best Paper Awards at international conferences.

Charles B. Tsang received a colon and rectal surgery fellowship and completed his postgraduate training at the University of Minnesota. His specialty and interests are transanal and edoscopic ultrasound, biosphincter substitutes in the surgical treatment of fecal incontinence, and pelvic floor physiology. He is currently as a senior consultant with the National University Hospital, Singapore.